Nanomechanical Characterization of Brittle Rocks

Annalisa Bandini, Paolo Berry, Edoardo Bemporad and Marco Sebastiani

Abstract After an introduction describing the indentation techniques traditionally applied to the study of micromechanical properties of minerals and rocks, phenomena induced by the diamond tip's penetration into crystalline rocks are analyzed. Crystalline rocks are characterized by low values of the critical breakage load, i.e. the threshold load corresponding to the transition from a ductile to a brittle behavior. As a consequence, it seems more convenient to examine the mechanical behavior of crystalline rocks by using instrumented nanoindentations. Above the critical load, ranging from rock to rock, fractures occur, affecting the indentation results and thus invalidating the values of the rock mechanical properties obtained by indentation data processing. In order to determine the correct values of the hardness and elastic modulus of brittle rocks, an innovative measurement modality for rocks, i.e. Continuous Stiffness Measurement mode, is proposed. By providing the continuous evolution of the hardness and of the elastic modulus as a function of the indentation depth, it has proven particularly suited to analyze the effects of induced fracturing on the load versus displacement curve.

1 Introduction

Crystalline rocks consist of crystals of the same mineral or of aggregates of several mineral grains and contain discontinuities of different nature. Simmons and Richter (1976) and Kranz (1983) classified such microdiscontinuities into four types:

- grain boundaries (following the contacts between the grains);
- intragranular (lying inside the grains and not contacting the boundaries);

A. Bandini (✉) · P. Berry
Department of Civil, Chemical, Environmental and Materials Engineering (DICAM), University of Bologna, via Terracini, 28, 40131 Bologna, Italy
e-mail: annalisa.bandini4@unibo.it

E. Bemporad · M. Sebastiani
Engineering Department, Roma Tre University, via della Vasca Navale 79, 00146 Rome, Italy

A. Tiwari (ed.), *Nanomechanical Analysis of High Performance Materials*, Solid Mechanics and Its Applications 203, DOI: 10.1007/978-94-007-6919-9_11,
© Springer Science+Business Media Dordrecht 2014

- intergranular (intersecting grain boundaries);
- multigranular (the longest cracks, crossing several grains and their boundaries).

At the scale of the laboratory specimen, crystalline rocks are considered mostly continuous and homogeneous media and, when there is a marked iso-orientation of the grains, anisotropic. For a detailed analysis at the microscopic scale, they are revealed as discontinuous solids, affected by a dense network of cracks and grain boundary cavities. Figure 1 shows some examples of microdiscontinuities in a granite's sample. More generally, the discontinuous nature and heterogeneity of rocks at the grain scale are well described in Blair and Cook (1998) and in Lan et al. (2010).

Depending on their distribution, nature and statistically prevailing orientation more than grains iso-orientation, the defects affect the rock's mechanical behavior at a varying extent.

The microdiscontinuities are surfaces along which the failure processes of the rock samples under critical state of stresses originate (Tapponnier and Brace 1976; Kranz 1979; Wong 1982). Consequently, to properly understand the mechanisms leading to the rock's macroscopic failure, analyses should be performed even at the micro and nanoscale (discontinuities scale), where the failure begins.

The micro and nano scale analysis on the rock's mechanical response highlights the clear influence of the above mentioned discontinuities on the indentations performed with the different methods available today. Indeed, unlikely the observations in metals, for instance, the impression's shape in rock samples completely differs from the geometry provided by the interpretative models, as it is generally characterized by an intense fracturing, by detachments of chips, wedges, that may give rise to unformed craters around the contact area between the sample and the indenter.

Despite the deviation, in terms of indent's shape, from experimentation and theoretical models, the mechanical properties (hardness and elastic modulus) are calculated assuming the rock as a continuous, isotropic or anisotropic medium. As a consequence, those values can be affected by significant errors, which can be due to the fact that the method does not consider the phenomena induced by the tip

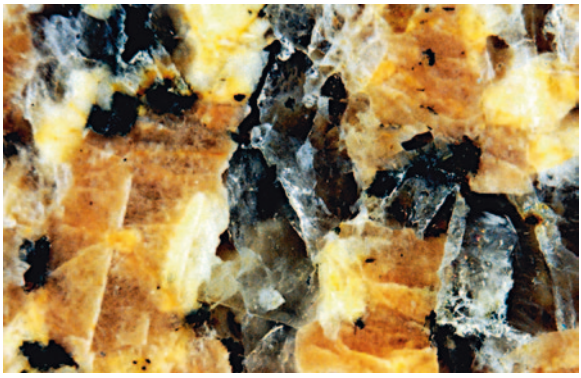

Fig. 1 Polished surface of a granite sample. Aggregates of quartz, feldspar and biotite can be recognized. In quartz the microcracks net clearly stands out, while in feldspars grains the cleavage planes traces are more obvious. In biotite some microcracks can be seen even at naked eye

penetration into the rock sample during loading and unloading, because the micro-discontinuities act as stress concentrators.

In order to investigate on the influence of the defects network on the mechanical behavior under indentation of rocks, instrumented Berkovich nanoindentations in Continuous Stiffness Measurement (CSM) mode were carried out. This modality, developed by Oliver and Pharr in 1992 to evaluate the elastic modulus and the hardness of continuous, isotropic and elasto-plastic materials, has been adopted for the first time for the study of rock materials by Bandini et al. (2012) to examine the relationships between the cracks net and the micromechanical parameters of brittle and discontinuous media, such as hard rocks.

In the rock mechanics literature, before the work of Bandini et al. (2012), instrumented indentation techniques were limited to the determination of micromechanical properties of rocks adopting the conventional quasi-static method, not in CSM modality (Broz et al. 2006; Whitney et al. 2007; Zhu et al. 2007; Mahabadi et al. 2012).

Compared to the conventional method, the CSM allows analyzing dynamically the mechanical behavior (hardness and elastic modulus) and the fracture mechanisms of materials during indentation, as a function of penetration depth with a spatial resolution of few nanometers, and consequently it is particularly suited to study the failure mechanisms of rock materials.

1.1 Conventional Indentation Methods for Rocks Characterization

In rock mechanics the most widespread indentation techniques are the not instrumented ones (Delgado et al. 2005; Xie and Tamaki 2007; Yilmaz 2011).

Not instrumented indentation is a static method involving applying and removing a specified load onto the sample surface by a diamond probe. The indentation measurements are taken after the indentation event.

The Knoop diamond tip is usually utilized in rocks, since, compared to the other indenters, has the advantage to produce an elongated and therefore easily measurable impression, also when the imprint tends to undergo cleavage deformation to be charged to the material brittleness, as occurs in many minerals and rocks.

The reference surface commonly used to calculate the Knoop hardness is the projected contact area (impression section), A_{PCA}, and the Knoop microhardness is determined with the Eq. (1):

$$\mathrm{HK} = \frac{\mathrm{P}}{\mathrm{A_{PCA}}} = \frac{\mathrm{P}}{\mathrm{L}^2} \cdot \frac{2}{\cot\left(\frac{\alpha}{2}\right) \cdot \tan\left(\frac{\beta}{2}\right)} = 14.229 \cdot \frac{\mathrm{P}}{\mathrm{L}^2} \tag{1}$$

where $\alpha = 172° \ 30'$ e $\beta = 130°$ are the two characteristic angles of the Knoop indenter tip, and P and L the load and the long diagonal's length of the impression.

The Vickers microhardness, instead, is conventionally calculated by considering, as reference surface, the true contact area, A_{TCA}, represented by the side surface of the pyramid, in accordance with the following equation:

$$HV = \frac{P}{A_{TCA}} = \frac{P}{\frac{d^2}{2 \cdot \sin(\phi/2)}} = 1.8544 \cdot \frac{P}{d^2} \quad (2)$$

where $\phi = 136°$ is the characteristic angle of the indenter, and P and d are the load and the diagonal length of the squared section impression.

In both Eqs. (1) and (2), hardness is determined purely from the measurements of the diagonals length of the permanent impression under a given load, irrespective of the impression's shape.

The impressions in rocks are rarely regular, sometimes fully developed, often partly developed and occasionally they are simply a cross mark. In performing Vickers indentations on coal, Das (1974) observed several times that impressions having nearly identical length of diagonals and consequently the same hardness according to Vickers formula had different shape of the impressions.

These remarks are also confirmed by the results obtained with other testing methods, including scratching and impact tests on rock samples (Berry et al. 1989; Beste et al. 2004).

The impressions shape in rocks are more complex than the models' geometry (Hughes 1986; Lindqvist and Hai-Hui 1983), valid for homogeneous and continuous media. Such complexity is due to the microstructural parameters, which play an important role: position, orientation according to the stress direction, frequency, size and type of discontinuities (cracks across mineral grains, mineral contacts, cracks crossing different species, cleavage planes), discontinuities' alteration degree, grains' mineralogical composition.

The theoretical models that describe the behavior of rocks under point loads are limited to consider the brittleness of homogeneous materials and then assume symmetrical shapes of the permanent impression, whereas they do not take into account the inhomogeneities also at the scale of the indenter's tip, which might cause distortions or asymmetries.

These models predict the formation of regular and symmetrical chips around the indenter (Paul and Sikarskie 1965; Pariseau and Fairhurst 1967; Lundberg 1974; Hughes 1986) and according to Paul and Sikarskie (1965), a zone of intense comminution is also created below the tip.

The models lead to conclude that for brittle materials, such as rocks, the contact area between the tip and the sample remains approximately constant from the beginning to the end of the test. It follows that in brittle rocks the impression is never the "negative" portion of the penetrated indenter ("positive").

The Eq. (1) and (2) give the hardness in terms of ratio between the applied load and the contact surface between the tip and the material under observation, assuming that the entire portion of the penetrated tip is in contact (hypothesis that is verified for ductile materials, but not for brittle rocks).

Thus, it may be reasonably assumed that the rocks' hardness values calculated according to Eqs. (1) and (2) are overestimated and each value deviates from the "true" value, in first approximation, proportionally to the induced effects (microcracking, craters, etc.), which vary point to point, as a function of the fabric conditions around the tip.

1.2 Rock's Indentation: Induced Phenomena

From examining the residual impressions on rock samples, it appears that the states of stress due to a shaped tip's penetration generate effects in an area much larger than the indenter's section, depending upon the rock's heterogeneity degree (pores and microcracks).

Cracks within each crystalline element, contact surfaces between grains of the same mineral or different species, schistosity surfaces and cleavage planes act as "weakness points" in the rock structure. As the microstructure's conditions of the rock change in the contact area between the rock sample and the indenter, various phenomena can be noted.

We may observe rock's plasticization, as pointed by the mark on the left side of the impression in Fig. 2a. The Fig. 2b shows a bifurcation of the impression, as well as another mark. The pictures c and d (Fig. 2) are characterized by more or less symmetrical marks of various extents. In the last two pictures of Fig. 2(e and f) two craters were generated next to the indent. Similar phenomena are visible even in Fig. 3 relating to indentations on feldspar grains of the same granite sample of Fig. 2. The two impressions in Fig. 3a are affected by intense streaks. Moreover, the Fig. 3 (b, c, d, e) gives examples of craters of varying shape and extension. The Fig. 3e displays an intense network of induced microfractures at the ends of the long diagonal of the impression.

The Fig. 4, referring to impressions on biotite grains, highlights the influence on the microstructure on the shape and extension of the induced effects. The indents with the longest diagonal parallel to the cleavage planes (Fig. 4a) are accompanied by a set of cracks parallel to the longest diagonal. It means that the biotite lamellae are widened under indentation. The indentations perpendicular to cleavage (Fig. 4b) induce the rock deformation up to cause a dense network of microcracks parallel to the short diagonal of the rhombus, giving to the indent a squatter shape. The impression produced along a direction slightly inclined (Fig. 4d) with respect to the configuration of Fig. 4a is markedly asymmetrical. It seems more pronounced toward the left side and such extension is clearly due to the lamellae orientation, which opens under stress.

In the same rock sample we can often find both regular and shapeless indents, surrounded by craters that make the diagonal's length difficult to measure and therefore alter the impression's shape. Figure 5 refers to the same Carrara marble sample. In the first case (Fig. 5a) a close net of well-marked microfractures extends both on the right and on the left side, but anyway the impression is very

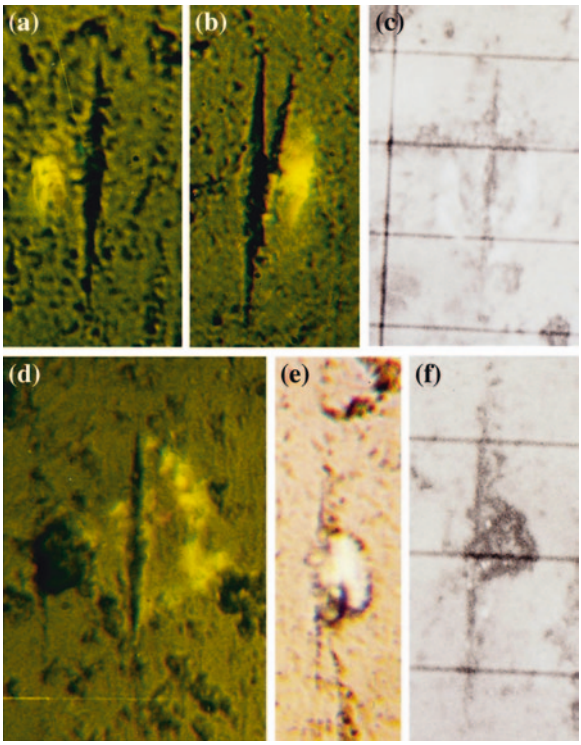

Fig. 2 Optical micrographs of Knoop residual impressions ($P = 1.9$ N) on quartz grains of a granite sample. The first four pictures (**a**, **b**, **c**, **d**) show signs of coaction or induced yielding. The pictures (**e** and **f**) depict the craters produced by the penetration of the indenter tip, from the edges of the impression

clear and visibly contrasts into the background. In the second case (Fig. 5b), it is not easy to define the exact contour of the impression since the detachment of a large piece of material occurred.

According to Brace (1961), the impression's shape should be clearer and more regular in extremely fine-grained rocks because the network of microcracks has a mesh less than or comparable with the tip size and the structural weakness is homogenously spread throughout the rock.

Generally, the effects of each indentation extend well beyond the contact area between the sample and the indenter tip. The failure does not occur with radial cracks, as assumed by the theoretical models and observed in other materials (Oliver and Pharr 1992). Fractures arise along preexisting microdiscontinuities. For instance, Wong and Bradt (1992) noted that indentations inside calcite crystals always induce cleavage cracks and twins, regardless of the tip's orientation with reference to the cleavage planes directions (Carter et al. 1993).

The indentation effects also depend on the mineralogical composition of the grains. The grooves produced by scratching within single grains are characterized by different shapes depending on the involved mineral species (Berry et al. 1989; Beste et al. 2004). For example, in Berry et al. (1989) the minerals of granite respond differently to the shear stresses. In the feldspar the groove appears to be

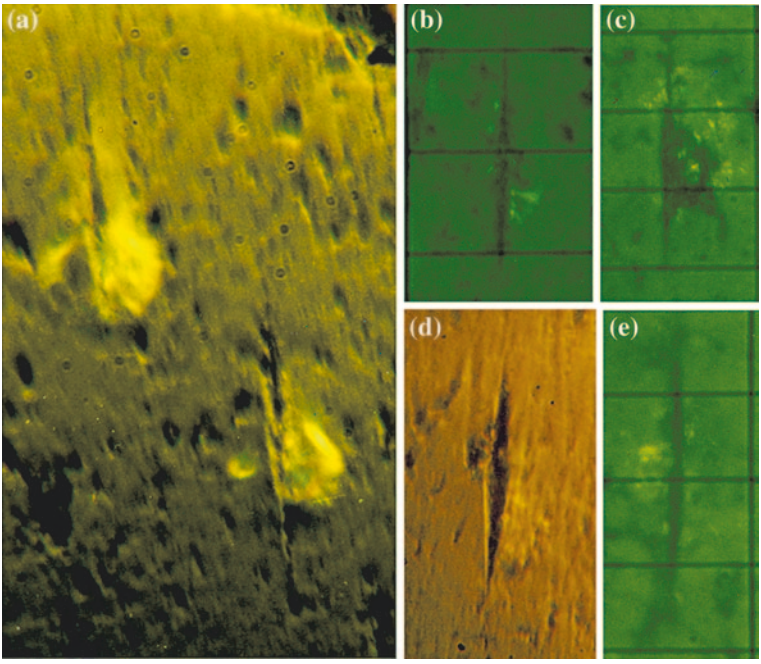

Fig. 3 Optical micrographs of Knoop residual impressions ($P = 1.9$ N) on feldspar grains of a granite sample. The first picture (**a**) shows marks of coaction or induced yielding (two impressions). The other four pictures (**b**, **c**, **d**, **e**) highlight microfracturing and micro-craters beyond the yielding signs

controlled by the induced cracks and it mainly develops along the cleavage planes. Sometimes the groove is barely detectable. In quartz the boundary is more irregular than in the feldspar, consisting of the microcracks produced by the cutter and by the preexisting ones. Moreover, along the grooves' boundaries a band of discontinuities can be noticed. In the biotite, the groove is contained inside the mineral and marked effects beyond the streak are not visible.

At the contacts between the various rock minerals, the effects vary in dependence of the species of neighboring minerals, of the size of the crystals elements, of the joint strength and of its orientation with respect to the groove. If the orientation is favorable compared to the stress direction, stresses concentrate in the flaws edges determining the propagation and coalescence along the preexisting discontinuities.

The extent and the intensity of the produced phenomena depend on the value of the applied load, in addition to the rock fabric. For example, a load of 2 N induces cracks in all the Mohs minerals (Broz et al. 2006). Each Mohs mineral responds differently to indentation, as is evident by the length, number, direction and type of cracks produced by Vickers microindentation (Broz et al. 2006).

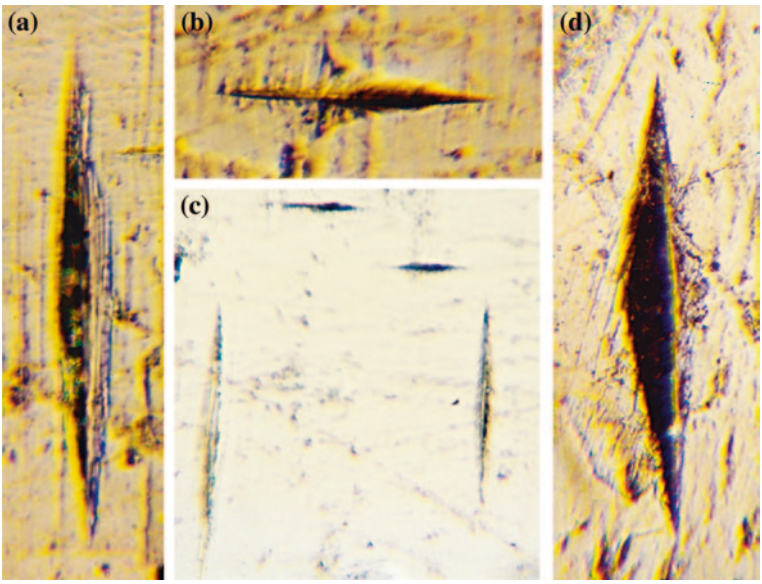

Fig. 4 Optical micrographs of Knoop residual impressions ($P = 1.9$ N) on biotite grains of a granite sample. Cleavage markedly affects the impression's shape and sizes. The first picture (**a**) shows effects induced by an indentation along the cleavage planes direction. The second one (**b**) represents the produced effects when the tip is rotated through 90° relative to the cleavage planes direction. The third one (**c**) compares the previous configurations. The last one (**d**) shows an impression produced by rotating the tip's longest diagonal by 18° with respect to the cleavage.

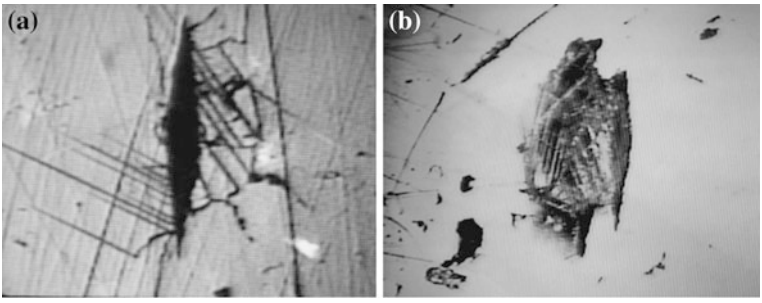

Fig. 5 Optical micrographs of two Knoop residual impressions ($P = 1.9$ N) on Carrara marble

In crystalline rocks induced cracking is evident also at lower loads. Figures 6 and 7 depict illustrative examples of Knoop and Vickers indents, by applying a load of 100 mN on a marble sample. Cleavage cracks and twins are clearly identifiable, despite the low applied load.

In Bandini et al. (2012) a load of a few mN is enough to have fracturing around the indents in marble. Likewise, also Skrzypczak et al. (2009) always noticed

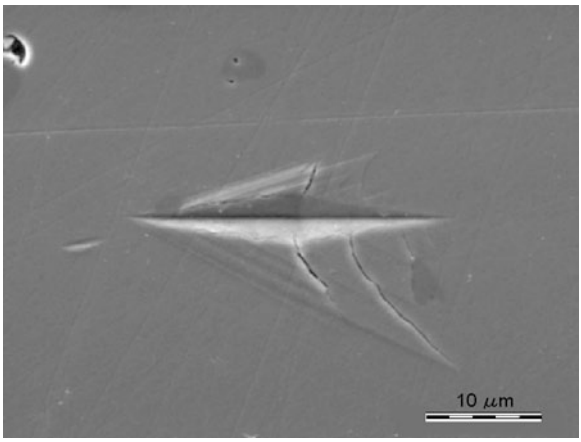

Fig. 6 SEM micrograph (2000x, SE) of a Knoop indent ($P = 100$ mN) into a calcite grain of a marble sample (Bandini et al. 2012)

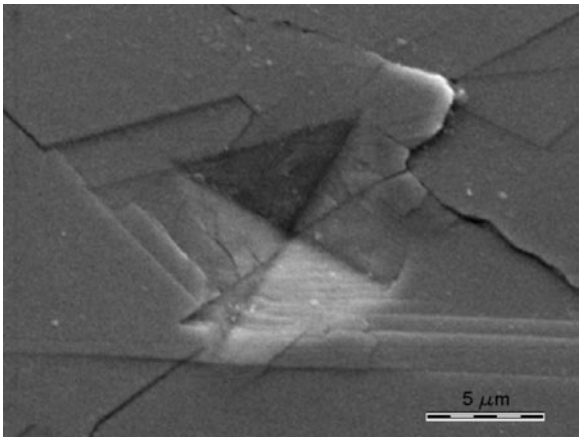

Fig. 7 SEM micrograph (5000x, SE) of a Vickers indent ($P = 100$ mN) into a calcite grain of a marble sample (Bandini et al. 2012)

cracks and were not able to experimentally observe the transition from plastic deformation to brittle fracture, because the range of applied loads (from 250 mN to 5 N) was higher than the threshold load between ductile and brittle response.

1.3 Critical Breakage Size

During an indentation, the energy given to the sample may be spent in two different ways. Fracturing occurs, as the energy allows creating new surfaces, or the material deforms plastically, the energy being dissipated by atoms rearrangement. In addition, a part of energy, which can be neglected, is dissipated as heat.

The one or the other of the two above mentioned phenomena prevails depending on the value of the applied load and, as a consequence, on the sizes of the indent produced by indentation.

The critical breakage size, a_{crit}, is defined as the size corresponding to the transition from a ductile to a brittle behavior. Consequently, it results from the energetic balance between plastic deformation and crack propagation.

In particular, the energy W_S needed to plastically deform a particle of volume a^3 can be expressed with the Eq. (3):

$$\mathrm{W_S} = \frac{\sigma_\mathrm{P}}{2 \cdot \mathrm{E}} \cdot \mathrm{a}^3 \tag{3}$$

where σ_P and E are, respectively, the yield stress and the Young's modulus of the material.

The energy W_P required to create a new surface a^2 is:

$$\mathrm{W_P} = \mathrm{G} \cdot \mathrm{a}^2 \tag{4}$$

where G is the crack propagation energy.

It results:

$$\mathrm{a_{crit}} = \frac{2 \cdot \mathrm{E} \cdot \mathrm{G}}{\sigma_\mathrm{P}^2} \tag{5}$$

The energy balance becomes favorable to plastic deformation for sizes lower than the critical one, a_{crit}. Above this size, the behavior becomes brittle and fractures occur.

Determining accurately the critical breakage size with Eq. (5) is complex, since it requires to know σ_P and G. On the other hand, the heterogeneity of the rock materials leads to a high dispersion in the values of such parameters and then it is difficult to choose the more appropriate values.

Skrzypczak et al. (2009) introduced a procedure to experimentally determine the critical breakage size through Vickers indentation techniques. This procedure consists in characterizing the indents by the diagonal length d of the plastically deformed area and by the length $2c$ of the cracks around the indent (Fig. 8).

The diagonal length d of the permanent impression is related to the Vickers hardness HV through Eq. (2).

The cracks length $2c$ depends on the material resistance to crack propagation. The fracture toughness under the fracture mode I, K_{IC}, can be calculated with Eq. (6):

$$K_{IC} = 0.016 \cdot \left(\frac{E}{H}\right)^{\frac{1}{2}} \frac{P}{c^{\frac{3}{2}}} \tag{6}$$

Assuming that E, HV and K_{IC} are independent of the applied load P, the two Eqs. (2) and (6) are represented by two straight lines of slope 2 and 3/2 respectively in the plot of Fig. 8b. Thus the intersection point obtained by extrapolating the two straight lines defines the critical load P_{crit} and the corresponding size a_{crit}.

For loads higher than P_{crit}, brittle cracks appear, while, for load lower than P_{crit}, only plastic deformation is observed. The a_{crit} corresponds to the critical size

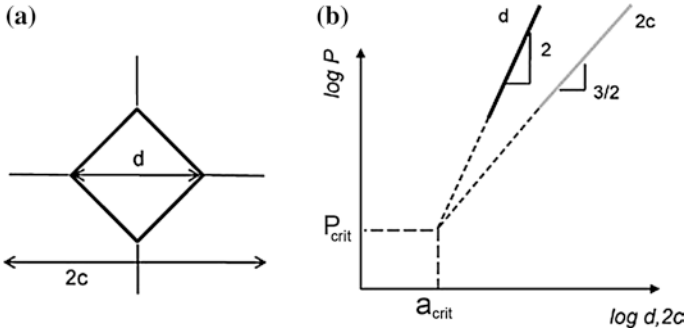

Fig. 8 **a** Scheme of a Vickers indent with radial cracks; **b** Theoretical evolution of the diagonal length *d* of the Vickers indentation and crack length *2c* versus the applied load *P* (Skrzypczak et al. 2009)

below which no cracking occurs. By applying this methodology, Skrzypczak et al. (2009) obtained low value for critical load and size (4-5 mN e 1.9 μm, respectively) in Carrara marble, suggesting that microindentation of crystalline rocks results in cracking.

2 Instrumented Nanoindentation in Continuous Stiffness Measurement Modality in Rocks

Compared to the not instrumented one, the instrumented indentation testing has the advantage of continuously measuring the penetration depth of the indenter into the sample surface and the load applied to the sample.

Unlikely the materials science where it is largely used, the instrumented indentation has been rarely utilized to study the micromechanical properties of minerals and rocks and never in CSM mode before the work of Bandini et al. (2012).

Broz et al. (2006) used nanoindentation to determine the mechanical properties of Mohs scale minerals. Whitney et al. (2007) reported the elastic modulus and hardness by instrumented indentations for common metamorphic minerals. Zhu et al. (2007) attempted to correlate the hardness and the elastic modulus maps of rocks samples (quartzite and granodiorite), by Berkovich nanoindentation, to the mineralogy and shape of the rocks-forming minerals grains, resulting from analysis with optical and scanning electron microscopies.

Mahabadi et al. (2012) conducted grid micro-indentation tests, to determine the instrumented indentation modulus and fracture toughness of the constituent phases of a crystalline rock as input parameters for numerical modeling. Such research represents one of the first attempts to consider the rocks heterogeneity when modeling their mechanical behavior.

The instrumented indentation testing was developed to measure the mechanical properties of a material from the indentation load and indentation depth data obtained during on cycle of loading and unloading. A tip is pushed into the sample surface. It produces a load versus displacement curve from which the indentation modulus and the hardness of the tested material can be quantified by following the method developed by Oliver and Pharr (1992, 2004).

2.1 Oliver and Pharr's Method

During an instrumented indentation, the indenter displacement h, relative to the initial undeformed sample surface, is continuously registered under the controlled application of a normal load P. h_{max} represents the displacement at the peak load P_{max}, h_C is the contact depth and is defined as the depth of the indenter in contact with the sample under load, h_f is the final displacement after complete unloading and S is the slope of the unloading curve defined as contact stiffness (Fig. 9).

During loading, deformation is supposed to be both elastic and plastic, since the permanent impression forms. During unloading, it is assumed that only the elastic displacements are recovered. For this reason, the method does not apply to materials in which additional plastic deformation is observed during unloading path of the load versus displacement curve, a phenomenon that is usually referred as "reverse plasticity". However, such events are very unusual and have been observed only in a few cases and only in case of metals (Oliver and Pharr 1992, 2004), so they can be considered as negligible in the investigated rock and more generally in rock materials.

The elastic nature of the unloading curve facilitates the analysis and the contact process can be modeled by using the Sneddon's elastic solution (Sneddon 1965).

The reduced modulus E_R, which takes into account elastic displacements occur in both the specimen and the indenter, describes the elastic contact between the indented material and the indenter's tip. It is calculated from the contact stiffness S

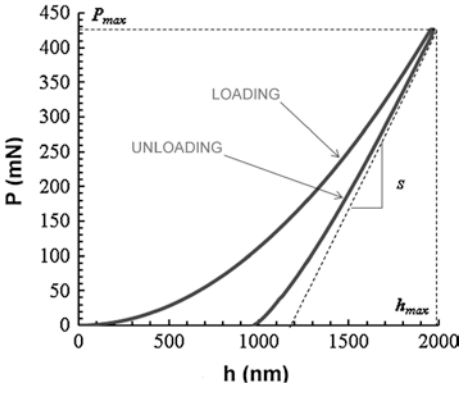

Fig. 9 A typical load P versus displacement h curve for a conical indenter

and the contact area A_C, by using the Eq. (7) derived from the Sneddon's solution (Sneddon 1965) for the elastic contact between a cone and a flat surface:

$$E_R = \frac{\sqrt{\pi}}{2 \cdot \beta} \cdot \frac{S}{\sqrt{A_C}} \tag{7}$$

where β is a constant depending on the indenter's geometry ($\beta = 1.034$ for a Berkovich indenter and $\beta = 1$ for a spherical tip).

Oliver and Pharr (1992) suggested the use of a power law to describe the unloading curve:

$$P = B \cdot (h - h_f)^m \tag{8}$$

where B and m are material constants determined by best fitting analysis ($1.2 \leq m \leq 1.6$).

The slope of the upper part of the unloading curve defines the contact stiffness S:

$$S = \left(\frac{dP}{dh}\right)_{h_{max}} = B \cdot m \cdot (h - h_f)^{m-1} \tag{9}$$

The contact area A_C can be calculated continuously from the depth of the indenter-sample contact h_C.

By applying the elastic model of Sneddon (1965), it follows:

$$h_C = h_{max} - \eta \cdot \frac{P_{max}}{S} \tag{10}$$

where the constant depends on the geometry of indentation and can be derived analytically from the Sneddon's solution ($\eta = 0.72$ for cones and $\eta = 0.75$ for spheres).

Therefore:

$$A_C = f(h_C) \tag{11}$$

where the function $f(h_C)$, known as area function, is calibrated using standard sample of amorphous silica (SiO_2). The indenter shape at the apex is complex and in nanoindentation the function area is well expressed by a polynomial relation:

$$A = a_0 \cdot h_C^2 + a_1 \cdot h_C + a_2 \cdot h_C^{1/4} + a_3 \cdot h_C^{1/3} + \ldots \tag{12}$$

By knowing the Poisson's ratio, the elastic modulus of the material E can be determined from the reduced modulus E_R, by the Eq. (13):

$$\frac{1}{E_R} = \frac{1 - \nu^2}{E} + \frac{1 - \nu_i^2}{E_i} \tag{13}$$

where E, E_i, ν e ν_i are Young's moduli and Poisson's ratios for the specimen and the indenter.

The material hardness is expressed as follows:

$$H = \frac{P_{max}}{A} \tag{14}$$

where A is the projected contact area at the peak load P_{max}.

2.2 Continuous Stiffness Measurement Modality

The CSM mode lies in superimposing a small sinusoidal oscillation on the primary loading signal and analyzing the resulting response of the system (Oliver and Pharr 1992). The loading curve can be seen as the superposition of a series of small cycles of loading and unloading, from each of which the elastic modulus and hardness to that value of load may be determined. The hardness and elastic modulus can be recorded as a continuous function of the surface penetration depth by continuous measurement of the dynamic contact stiffness.

By providing the continuous evolution of the elastic modulus and hardness during the loading phase, the CSM allows to assess the critical load P_{crit} and, as a consequence, until which load value the elastic modulus and the hardness may be considered actually representative of the material.

2.3 Case Study

The experimentation has been carried out on a calcitic marble (Bandini et al. 2012; Bandini and Berry 2013), in which the granoblastic (with regular grains and triple points) and xenoblastic (with well interlocked grains of irregular shape) textures coexist. Such textures show a different response to stresses (Table 1) at the laboratory's scale even if the mineralogical composition is almost monomineralic and the grain size does not vary substantially as a function of microstructure.

Berkovich nanoindentations in CSM mode were performed inside calcite grains composing the two textures (xenoblastic and granoblastic) in order to examine the evolution of the indentation hardness, elastic modulus and fracture mechanisms of the two marble textures.

The experimental results show failure occurs from preexisting flaws, acting as stress concentrators in controlling the rock's strength.

Indentations cause the brittle failure of the calcite grains, whatever their shape (regular for granoblastic and irregular for xenoblastic one) and the induced fracturing is ruled by the cleavage planes (Fig. 10).

Such intragranular failures can be recognized by the load versus indentation depth curves and by the SEM micrographs of the indents (Fig. 11). These curve are never regular and in the loading part (Fig. 11a) often exhibit pop-in phenomena, i.e. sudden discrete increase of the penetration depth at an approximately

Table 1 Mechanical properties of the marble under investigation (Bandini et al. 2012)

		N	Min	Max	m	Δm^*(%)	v (%)
n [%]	X	6	3.2	2.9	3.5	\	6.3
	G	11	3.2	2.9	3.4		4.9
σ_c [MPa]	X	4	87.5	104.0	94.3	34.0	6.9
	G	4	60.8	72.0	66.9		6.3
σ_t [MPa]	X	3	7.3	8.8	8.1	33.1	7.5
	G	3	5.4	6.1	5.8		5.2
$V_{p,dry}$ [m/s]	X	6	5,446	5,296	5,616	60.5	1.9
	G	11	2,538	2,233	3,009		8.3
$V_{p,sat}$ [m/s]	X	6	6,136	6,108	6,175	7.8	0.4
	G	11	5,679	5,638	5,709		0.4

$^*\Delta m = \frac{|mX-mG|}{(mX+mG)/2} \cdot 100$

X xenoblastic; *G* granoblastic; *n* total porosity; σ_c UCS; σ_t Brazilian indirect tensile strength; $V_{p,dry}$ and $V_{p,sat}$ dry and saturated P-waves velocities; *N* number of tests; *min* minimum value; *max* maximum value; *m* mean value; Δm^* relative difference, in percent, between the mean values of xenoblastic and granoblastic parameters (mX, mG); ν variation coefficient

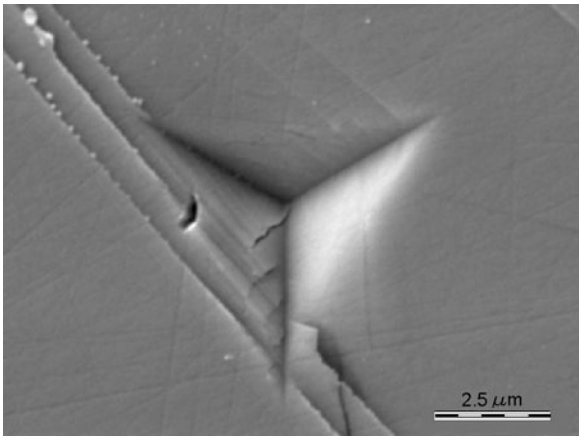

Fig. 10 SEM micrograph (10.000×) of a Berkovich indenter: fracturing induced by the tip penetration (Bandini et al. 2012)

constant load, as also noticed in other materials (Jian 2007; Saber-Samandari and Gross 2009; Tulliani et al. 2009). The pop-in is due to the formation of cracks, fractures around the indenter, as found by Presser et al. (2010), because of the rock inhomogeneity even on the scale of hundreds of nanometers.

Cracks are noted around each indent and the transition from plastic deformation to brittle fracture cannot be directly observed because the range of the maximum applied loads appears higher than the plastic-brittle threshold of calcite.

The fracturing induced by the indenter's penetration into the sample causes the progressive decrease of the elastic modulus and of the hardness, continuously recorded during loading (CSM mode) (Fig. 12).

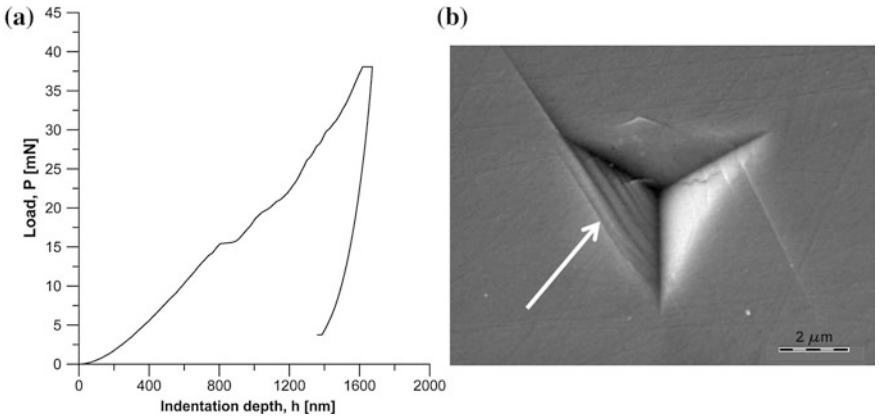

Fig. 11 Berkovich nanoindentations. **a** Load P versus indentation depth h; **b** SEM micrograph (10.000×) of the impression generated by the indentation, where fracturing is indicated by an arrow (Bandini et al. 2012)

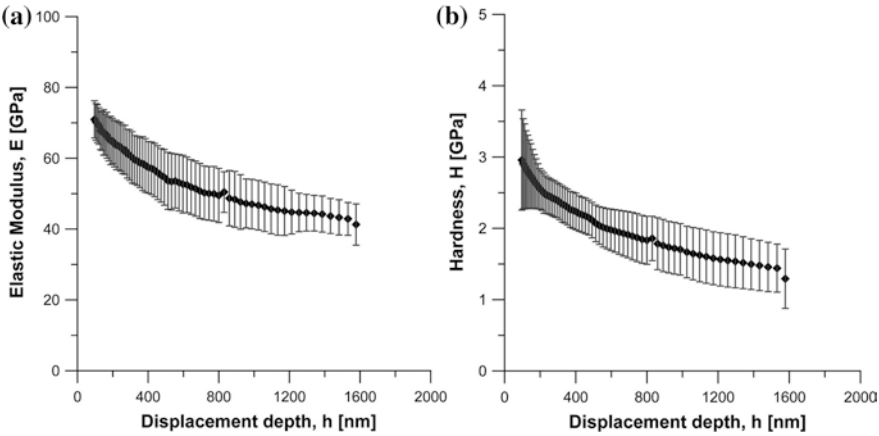

Fig. 12 Elastic modulus E (**a**) and Berkovich hardness H (**b**) variations during an indentation (nanoindentations in displacement control, CSM mode)

Actually, they should be considered as apparent elastic modulus and hardness, since such reduction appears due not to actual variations of the calcite grains properties but to failure and sliding along the cleavage planes of calcite grains.

The elastic modulus and the hardness obtained by the conventional instrumented indentation (without applying the CSM mode) correspond to the values at the deepest penetration depth, i.e. E_{max} (Fig. 13) and H_{max}.

For the extensive cracking during loading which reduces the apparent elastic modulus and hardness during indentation, E_{max} and H_{max} would be affected by

a significant error and consequently the conventional instrumented indentation would give a wrong description of the rock properties.

On the other hand, the CSM mode, giving the complete elastic modulus and hardness versus indentation depth profiles, allows to correctly estimating the rock properties.

As cracking is not observed for low applied loads (in this case, lower than 3 mN), the correct values of the elastic modulus and of the hardness can be achieved by extrapolating these profiles to zero depth (E^* and H^*) (Fig. 13), for

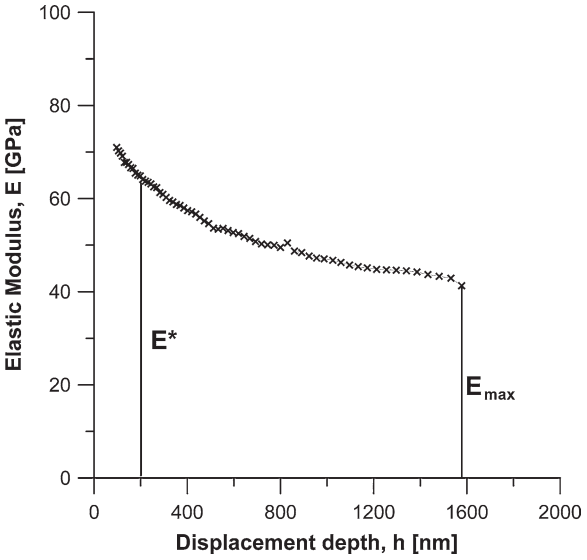

Fig. 13 Berkovich nanoindentations in CSM mode: elastic moduli extrapolated at zero depth (E^*) and to the maximum applied load (E_{max})

Table 2 Berkovich nanoindentations in CSM mode on xenoblastic marble: elastic modulus and hardness values extrapolated at zero depth (E^* and H^*) and at the maximum applied load (E_{max} and H_{max}) (Bandini et al. 2012)

	E* [GPa]	H* [GPa]	E_{max} [GPa]	H_{max} [GPa]
m [GPa]	75.0	3.4	42.3	1.4
ν (%)	6.0	9.1	10.4	28.4

instance, by fitting the profiles with a polynomial function. As can be seen, such values differ from the mechanical properties at the maximum load, E_{max} and H_{max} (Tables 2 and 3).

It results the calcite grains forming the two textures have the same intrinsic properties, for instance an elastic modulus of around 70 GPa (Fig. 14) in agreement with literature data for calcite (Broz et al. 2006; Presser et al. 2010), as we can see by the comparison of the curves of the elastic modulus versus

Table 3 Berkovich nanoindentations in CSM mode on granoblastic marble: elastic modulus and hardness values extrapolated at zero depth (E^* and H^*) and at the maximum applied load (E_{max} and H_{max}) (Bandini et al. 2012)

	E* [GPa]	H* [GPa]	E_{max} [GPa]	H_{max} [GPa]
m [GPa]	73.9	3.7	57.3	1.7
ν (%)	9.7	19.4	7.3	11.1

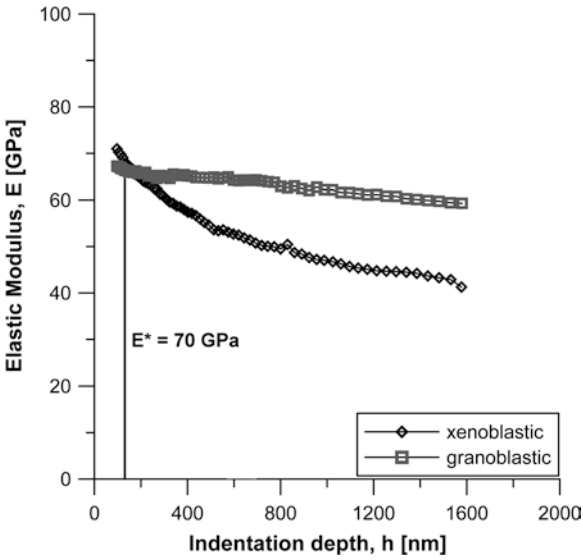

Fig. 14 Elastic modulus E versus indentation depth h: comparison between two calcite grains of xenoblastic and granoblastic marble

indentation depth (Fig. 14), which show no significant variation for depth lower than 200 nm.

Moreover, the CSM Berkovich nanoindentations picked out a more marked tendency to cleavage fracture of the xenoblastic marble grains, since the elastic modulus decreases more significantly with increasing the indentation depth (Fig. 14).

The calcite grains of the xenoblastic marble, which shows higher strengths at the scale of the laboratory sample (Table 1), appear more brittle than the calcite grains of the granoblastic texture and fracturing is already noticeable to a load of 5 mN, critical threshold load for the transition between plastic deformation and brittle fracture, similar to the value obtained by Skrzypczak et al. (2009) in Carrara marble.

With increasing the indentation depth, the elastic modulus of the calcite grains decreases more markedly in the xenoblastic marble, for a more significant tendency to cleavage fracture. It explains why we obtained lower elastic moduli at the maximum applied load, E_{max}, in the xenoblastic marble (Tables 2 and 3).

The same considerations can be made for the hardness. Similarly, the Berkovich hardness decreases more significantly in the calcite grains of the xenoblastic texture, resulting in lower apparent hardness (Tables 2 and 3), for the same reason.

3 Discussion

The study clearly shows that reliable values of the elastic modulus and hardness of rock materials can be obtained only after a careful analysis of the load versus displacement curve and of profiles of the elastic modulus and hardness during indentation (CSM mode). On the other hand, the conventional instrumented indentation does not take into account the tendency to brittle failure of the rock material. As a consequence, it can significantly underestimate the rock's mechanical properties, since the induced cracking determines a gradual decrease of the indentation modulus and hardness. The CSM allows to evaluate to which load value only plastic deformation occurs and the rock's hardness can be defined. Above the critical load, from rock to rock, fractures occur, affecting the indentation results and thus invalidating the values of the rock mechanical properties. The correct values of the elastic modulus and hardness can be achieved only for loads lower than the critical load. In the case study, indentantion results in cracking also at loads of few mN. As a consequence, the correct values of the elastic modulus and hardness can be achieved by extrapolating their profiles to zero depth.

4 Concluding Remarks

In rock mechanics the Knoop and Vickers not instrumented indentations are traditionally adopted. Because of the discontinuous nature of rocks, the residual impression produced by microindentation is almost never perfectly regular and several phenomena (fracturing, chips and wedges detachment, craters formation) are induced by the tip's penetration into a rock sample. Consequently, the calculated hardness deviates from the "true" value, proportionally to the induced effects.

The critical breakage load of crystalline rocks, corresponding to the transition from a ductile to a brittle behavior, is low (order of few mN). In other words, a load of few mN is enough to generate fractures around the impression. Therefore, it is more convenient to examine the mechanical behavior of such rocks by using instrumented nanoindentations. Above the critical load, ranging from rock to rock, fracturing occurs, affecting the indentation results, thus invalidating the values of the elastic modulus and hardness by instrumented indentation data processing. The research work proposed an innovative approach in rock mechanics, consisting in nanoindentation in continuous stiffness measurement (CSM) mode, to determine the correct elastic modulus and hardness of the rock.

By using the CSM modality, which provides the continuous evolution of the hardness and of the elastic modulus as a function of the indentation depth, the correct mechanical properties of the rock can be deduced by analyzing the effects of the induced fracturing on the load versus displacement curve. In the investigated rock, the hardness and elastic modulus may be obtained by extrapolating their profiles (CSM) during indentation, to zero depth. Moreover, the research shows

that, on the other hand, the mechanical properties by the conventional instrumented indentation, without applying the CSM, neglecting the fracturing's effect, cannot be considered as representative of the rock (apparent elastic modulus and hardness).

In conclusions, the study should be seen as a preliminary investigation aimed at evaluating the research opportunities offered by the application of the Oliver and Pharr's method to the rocks and, in particular, of the CSM mode for determining the mechanical properties of rock materials.

The theme deserves further investigations aimed at studying the micromechanical properties of soft rocks through instrumented indentation technique in CSM modality.

References

Bandini A, Berry P (2013) Influence of marble's texture on its mechanical behavior. Rock Mech Rock Eng 46(4):785–799

Bandini A, Berry P, Bemporad E, Sebastiani M (2012) Effects of intra-crystalline microcracks on the mechanical behavior of a marble under indentation. Int J Rock Mech Min Sci 54:47–55

Berry P, Bonifazi G, Fabbri S, Pinzari M (1989) Technological problems in cutting granite. In: MMIJ/IMM (ed) Proceedings of MMIJ/IMM joint symposium: today's technology for the mining and metallurgical industries, Kyoto, 2–4 October 1989, pp 215–227

Beste U, Lundvall A, Jacobson S (2004) Micro-scratch evaluation of rock types-a means to comprehend rock drill wear. Tribol Int 37(2):203–210

Blair SC, Cook NGW (1998) Analysis of compressive fracture in rock using statistical techniques: Part II. Effect of microscale heterogeneity on macroscopic deformation. Int J Rock Mech Min Sci 35(7):849–861

Brace WF (1961) Dependence of fracture strength of rocks on grain size. In: Proceedings 4th symposium on rock mechanics, Pennsylvania State University, pp. 99–103

Broz ME, Cook RF, Whitney DL (2006) Microhardness toughness, and modulus of Mohs scale minerals. Am Mineral 91:135–142

Carter GM, Henshall JL, Wakeman RJ (1993) Knoop hardness and fracture anisotropy of calcite. J Mater Sci Lett 12:407–410

Das B (1974) Vicker's hardness concept in the light of Vicker's impression. Int J Rock Mech Min Sci Geom Abstr 11:85–89

Delgado NS, Rodríguez-Rey A, Suárez del Río LM, Díez Sarriá I, Calleja L, Ruiz de Argandona VG (2005) The influence of rock microhardness on the sawability of Pink Porrino granite (Spain). Int J Rock Mech Min Sci 42:161–166

Hughes HM (1986) The relative cuttability of coal-measures stone. Min Sci Technol 3:95–109

Jian S-R (2007) Mechanical deformation induced in Si and GaN under Berkovich nanoindentation. Nanoscale Res Lett 3:6–13

Kranz RL (1979) Crack growth and development during creep of Barre granite. Int J Rock Mech Min Sci 18:23–35

Kranz RL (1983) Microcracks in rocks: a review. Tectonophysics 100:449–480

Lindqvist PA, Hai-Hui L (1983) Behaviour of the crushed zone in rock indentation. Rock Mech Rock Eng 16:199–207

Lan H, Martin CD, Hu B (2010) Effect of heterogeneity of brittle rock on micromechanical extensile behavior during compression loading. J Geophys Res 115:B01202

Lundberg B (1974) Penetration of rock by conical indenters. Int J Rock Mech Min Sci Geomech Abstr 11(6):209–214

Mahabadi OK, Randall NX, Zong Z, Grasselli G (2012) A novel approach for micro-scale characterization and modeling of geomaterials incorporating actual material heterogeneity. Geophys Res Lett 39:L01303

Oliver WC, Pharr GM (1992) An improved technique for determining hardness and elastic modulus using load and displacement sensing indentation experiments. J Mater Res 7:1564–1583

Oliver WC, Pharr GM (2004) Measurement of hardness and elastic modulus by instrumented indentation: advances in understanding and refinements to methodology. J Mater Res 19:3–20

Pariseau WG, Fairhurst C (1967) The force-penetration characteristic for wedge penetration into rock. Int J Rock Mech Min Sci 4(2):165–180

Paul B, Sikarskie DL (1965) A preliminary theory of static penetration by a rigid wedge into a brittle material. Trans Soc Mining Eng 232:372–383

Presser V, Gerlach K, Vohrer A, Nickel K, Dreher W (2010) Determination of the elastic modulus of highly porous samples by nanoindentation: a case study on sea urchin spines. J Mater Sci 45:2408–2418

Saber-Samandari S, Gross KA (2009) Micromechanical properties of single crystal hydroxyapatite by nanoindentation. Acta Biomater 5:2206–2212

Simmons G, Richter D (1976) Microcracks in rocks. In: Sterns RGJ (ed) The physics and chemistry of minerals and rocks. Wiley-Interscience, New York, pp 105–137

Skrzypczak M, Guerret-Piecourt C, Bec S, Loubet JL, Guerret O (2009) Use of a nanoindentation fatigue test to characterize the ductile–brittle transition. J Eur Ceram Soc 29:1021–1028

Sneddon IN (1965) The relation between load and penetration in the axisymmetric Boussinesq problem for a punch of arbitrary profile. Int J Eng Sci 3:47–57

Tapponnier P, Brace WF (1976) Development of stress-induced microcracks in Westerly Granite. Int J Rock Mech Min Sci Geomech Abstr 13(4):103–112

Tulliani JM, Bartuli C, Bemporad E, Naglieri V, Sebastiani M (2009) Preparation and mechanical characterization of dense and porous zirconia produced by gel casting with gelatin as a gelling agent. Ceram Int 6:2481–2491

Whitney DL, Broz M, Cook RF (2007) Hardness, toughness, and modulus of some common metamorphic minerals. Am Mineral 92:281–288

Wong TF (1982) Micromechanics of faulting in Westerly granite. Int J Rock Mech Min Sci 19:49–64

Wong TY, Bradt RC (1992) Microhardness anisotropy of single crystals of calcite, dolomite and magnesite on their cleavage planes. Mater Chem Phys 30:261–266

Xie J, Tamaki J (2007) Parameterization of micro-hardness distribution in granite related to abrasive machining performance. J Mater Process Technol 186:253–258

Yılmaz N (2011) Abrasivity assessment of granitic building stones in relation to diamond tool wear rate using mineralogy-based rock hardness indexes. Rock Mech Rock Eng 40:725–733

Zhu W, Hughes JJ, Bicanic N, Pearce CJ (2007) Nanoindentation mapping of mechanical properties of cement paste and natural rocks. Mater Charact 58:1189–1198